



science.sciencemag.org/cgi/content/full/science.aav7908/DC1

Supplementary Material for

Slowdown in Antarctic mass loss from solid Earth and sea-level feedbacks

E. Larour*, H. Seroussi, S. Adhikari, E. Ivins, L. Caron, M. Morlighem, N. Schlegel

*Corresponding author. Email: eric.larour@jpl.nasa.gov

Published 25 April 2019 as *Science* First Release

DOI: 10.1126/science.aav7908

This PDF file includes:

Materials and Methods

Figs. S1 to S19

References



Supplementary Materials for

Slowdown in Antarctic Mass Loss from Solid Earth and Sea-Level Feedbacks

E. Larour, H. Seroussi, S. Adhikari, E. Ivins,
L. Caron, M. Morlighem & N. Schlegel
correspondence to: eric.lrour@jpl.nasa.gov

This PDF file includes:

Materials and Methods

Figs. S1 to S19

References 42 to 48

The research was carried out at the Jet Propulsion Laboratory, California Institute of Technology, under a contract with the National Aeronautics and Space Administration.
© 2019. All rights reserved.

Materials and Methods

For RSL computations we rely on the mesh-based unstructured sea-level formulation SeSAW (Solid Earth and Sea-level Adjustment Workbench (29)) as implemented in the Ice Sheet System Model (ISSM (28)). For the Antarctic ice sheet, we rely entirely on the modeling capabilities of ISSM, which capture mass transport, stress balance (using the order 2D SSA approximation (42)) and high-resolution sub-element GLD (11). In terms of atmospheric forcing we apply a constant yearly surface mass balance corresponding to an average between 1979 and 2010, from the Regional Climate Model RACMO2.1 (43). For the ocean forcing, we use a melt-rate parameterization calibrated against the MITgcm ocean circulation model (11) and generalize it to all Antarctica ice shelves using already available computed melt rates (35) and existing knowledge of sub-ice-shelf cavity shapes. The ice-sheet model is initialized using an instantaneous spin-up of a 2D SSA model where basal friction is inverted for (28, 44) from InSAR surface velocities (10). This spin-up is carried out to match the configuration of Antarctica in terms of surface velocity and ice thickness in year 2000 (10). The thermal regime of the ice sheet is assumed steady-state (45) and the rheology of the ice dependent on an Arhenius type law (46). For ice shelves, where the rheology is poorly known, an inversion using observed velocities is carried out (47). The model itself is run in 2D, because 3D higher-order models such as the Blatter/Pattyn (48) are too computationally expensive for a 500 year 1-50 km resolution model. For the bed topography, which is essential to the stability of the spin-up, we cover the model domain

over the entire AIS as observed today, and interpolate its geometry from the Bedmap2 dataset, with specific exception to the Amundsen Sea sector, Recovery Ice Stream, and Totten Glacier. In these areas, we combine ice thickness data from ice penetrating radar, satellite derived ice velocities and surface mass balance from a regional climate model to map the bed at 150 m spatial resolution using the mass conservation (MC) approach (44) previously adapted to the Amundsen Sea Sector (10). For the surface topography, we rely on a dataset consistent with the MC approach (44). To account for the numerical shock in the instantaneous spin-up, we carry out a quick relaxation of 1 year before letting the transient model fully evolve in time.

Both the RSL and ice-sheet model are coupled on the same unstructured mesh, shown in Fig. S19. At the global level, this mesh is built using the GMSH anisotropic mesher, and refined to exactly capture the crude GSHHG coastline (Global Self-consistent, Hierarchical, High-resolution Geography Database, c-L1 coastlines (41)). The resolution of the mesh ranges from 30 km at the coast to 1600 km far offshore (see Fig. S19a and S19b). For Antarctica, where ISSM's ice-flow model is run, mesh resolution is refined for 18 independent basins (Fig. S19c). Each basin is meshed adaptively to best capture InSAR surface velocities (10, 12), leading to a mesh resolution of 2 km near ice-stream shear margins to 50 km inland. For the areas of WAIS, mesh resolution is significantly increased to vary from 1 km at the present-day grounding line, to 8 km upstream towards the bedrock trough (Fig. S19d). In addition, the entire area comprised between the year 2000 and year 2500 grounding line of TG is meshed at 1 km resolution (to satisfy the 1 km GLD criterion). The Antarctica mesh comprises a total of 221,266 elements. The global mesh comprises 412,364 elements (from which 375,192 are in Antarctica). Because mesh resolution and computational requirements are significant (each model run takes 4 days on 180 CPUs of the NASA AMES Pleiades cluster), the RSL model is only run at time intervals of 10 years. The ice-sheet model is run on each of the 18 basins of Antarctica at a time interval of 14 d. Every 10 years, ice thickness changes for every glaciated area of the Earth (including the 18 Antarctica basins) are used to compute a new RSL. In turn, this new RSL is transferred to the glaciated areas for use as boundary conditions to the ice-flow model, at the calving front (sea-level) and at the ice/bed interface to update the bedrock topography. Here, only AIS is computed interactively on a basin by basin basis. Stress-balance coupling at the ice divides is not implemented, as the resulting model would be too computationally prohibitive. However, this implies that thickness and stress-balance differentials at the ice divides develop after several hundred years. These jumps are significant between WAIS, Ronne and Ross Ice Shelf tributaries. We therefore decided to expand the mesh domain for WAIS to include the Ronne and Ross basins (resulting in 16 basins in Antarctica). For other basins, the differentials that developed did not exceed 10 m.

For all other glaciated areas, such as Greenland or Alaska, mass transport is constrained to match GRACE mass trends from 2003 to 2016, and extrapolated in time for every year starting model year 2000 (26). No attempt is made at modeling the stress balance, calving front and grounding line dynamics of these areas. The respective sea-level fingerprints of each of these glaciated areas can be seen in Figures 3 and S18 at year 2350. Given the impact the two-way coupling has on the evolution of Antarctica, we decided to validate our interval of 10 years in the computation of RSL, by exploring the impact of a larger or smaller time step. Fig. S10 shows that the optimal value is 5 years,

but that 10 years is acceptable if a grounding line position error margin of less than 10 km is desired.

Supplementary References and Notes:

42. D. MacAyeal, J. Geophys. Res. 94, 4071 (1989).
43. J. T. M. Lenaerts, M. R. van den Broeke, W. J. van de Berg, E. van Meijgaard, P. K. Munneke, Geophys. Res. Lett. 39, 1 (2012).
44. M. Morlighem, et al., Geophys. Res. Lett. 38, 1 (2011).
45. E. Larour, M. Morlighem, H. Seroussi, J. Schiermeier, E. Rignot, J. Geophys. Res. - Earth Surface 117, 1 (2012).
46. J. Glen, Proc. R. Soc. A 228, 519 (1955).
47. E. Larour, E. Rignot, I. Joughin, D. Aubry, Geophys. Res. Lett. 32, 1 (2005).
48. F. Pattyn, J. Geophys. Res. 108, 1 (2003).

Supplementary Figures

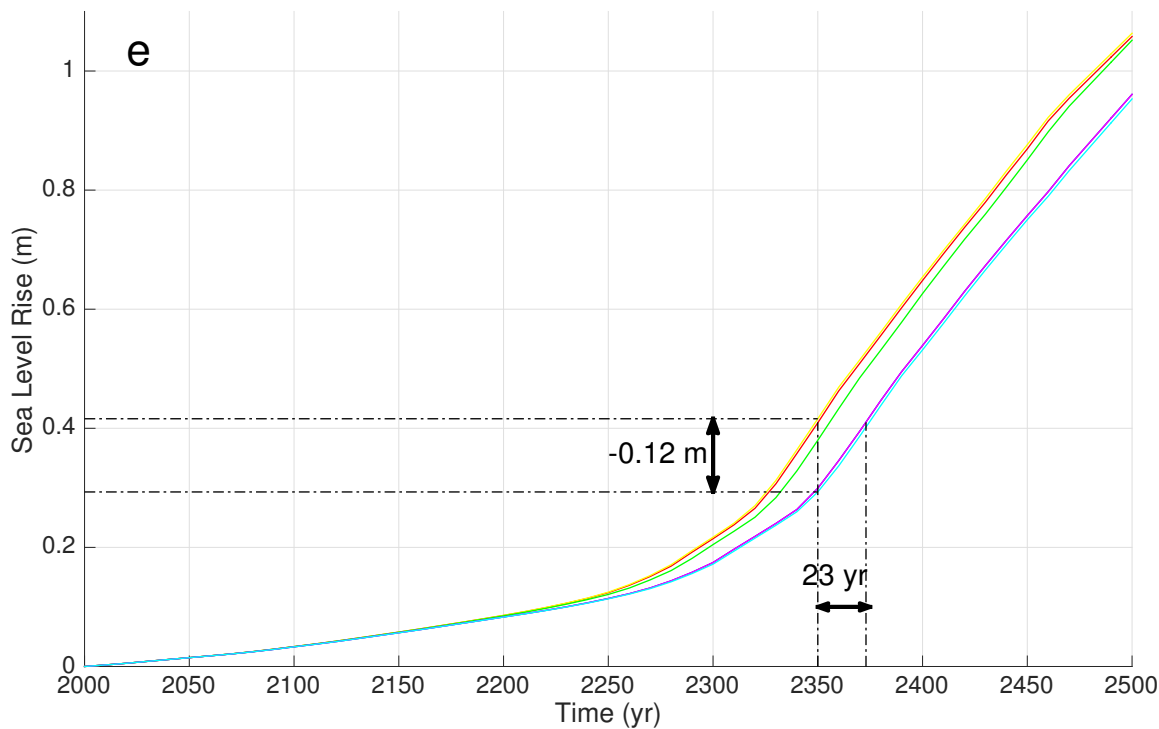


Fig. S1. 500 year contribution of TG to SLR (in m SLR equivalent). This figure is identical to Figure 5 except for the x-axis which here represents time (in yr) from the start of the control run at 2000 to the arbitrary end of the run which at 2500. Approximately 0.42 m SLR is achieved at 2350 with the UNC run, whereas including all solid-Earth processes, the same amount of SLR is only achieved 23 years later.

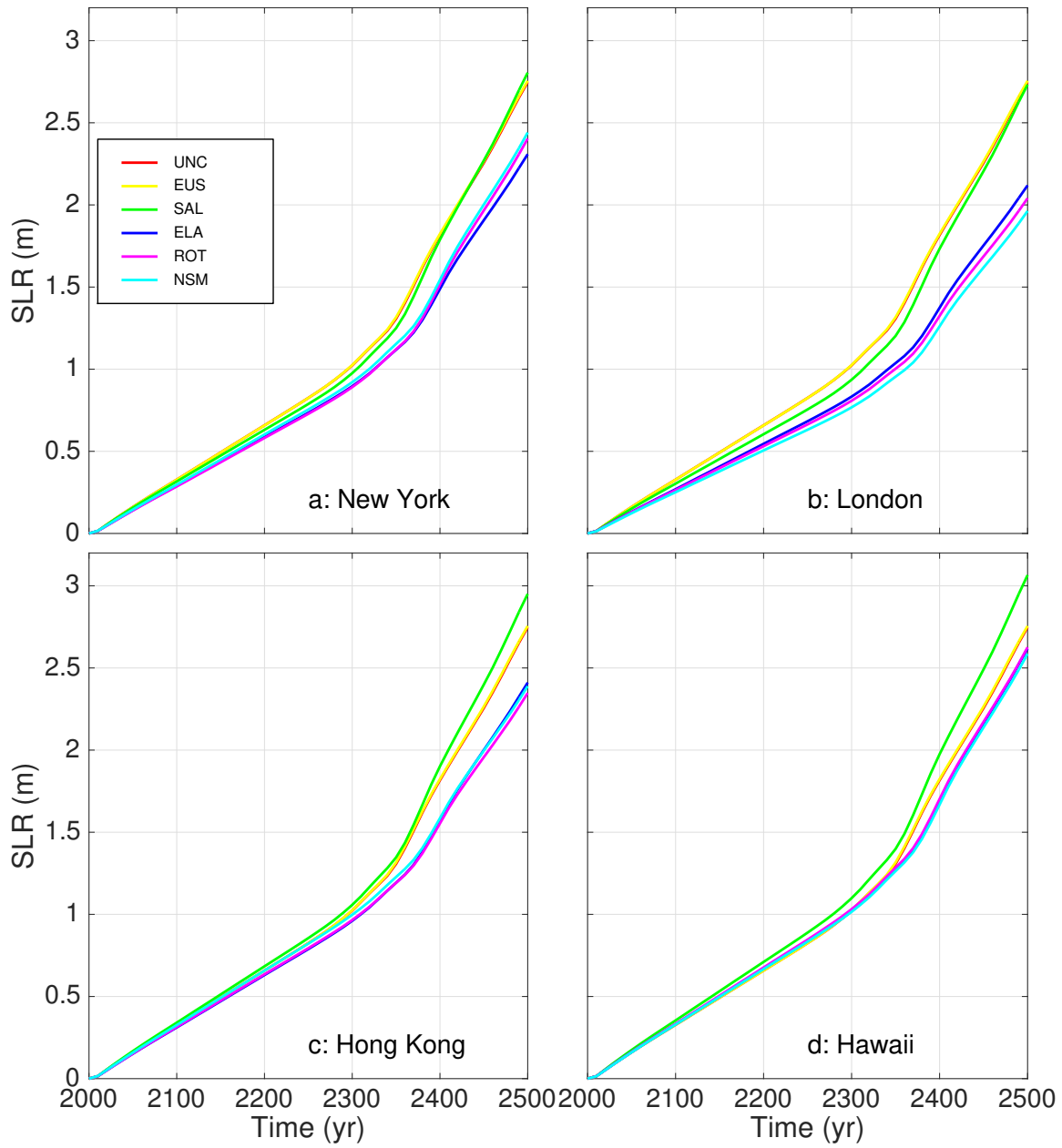


Fig. S2. 500 years of RSL projection for four cities around the world (in m). Results correspond to the six models defined in Table 1 for New York (a), London (b), Hong Kong (c) and Hawaii (d).

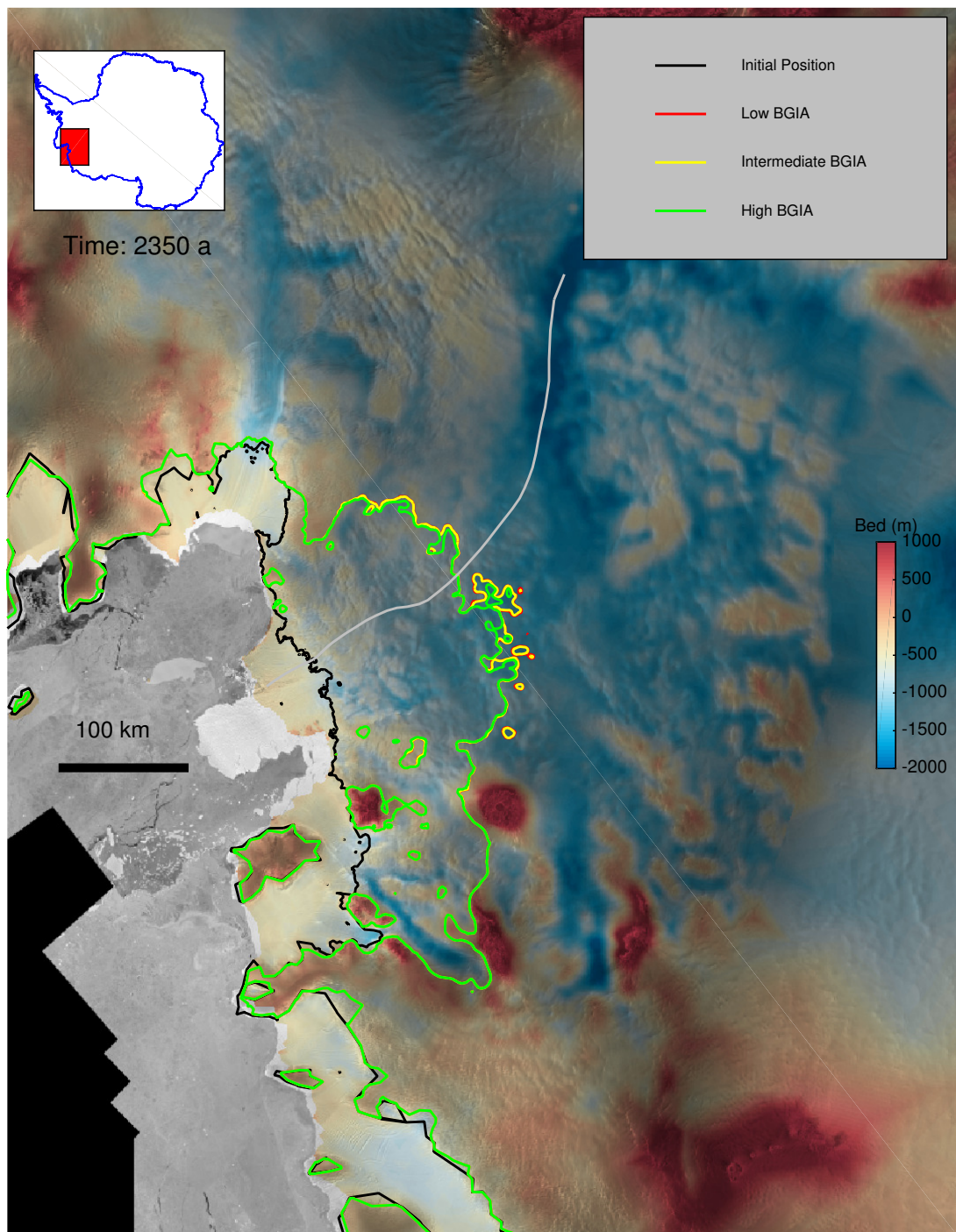


Fig. S3. Sensitivity of grounding-line migration to BGIA for the WAIS area. Three projections at 2350 of the grounding line position of WAIS are displayed for three different BGIA models (see Table 1 and main text for a description of this sensitivity experiment). The initial grounding line position in 2000 is shown in black. Grounding line positions are overlaid on a local bedrock topography of the continent (see Methods).

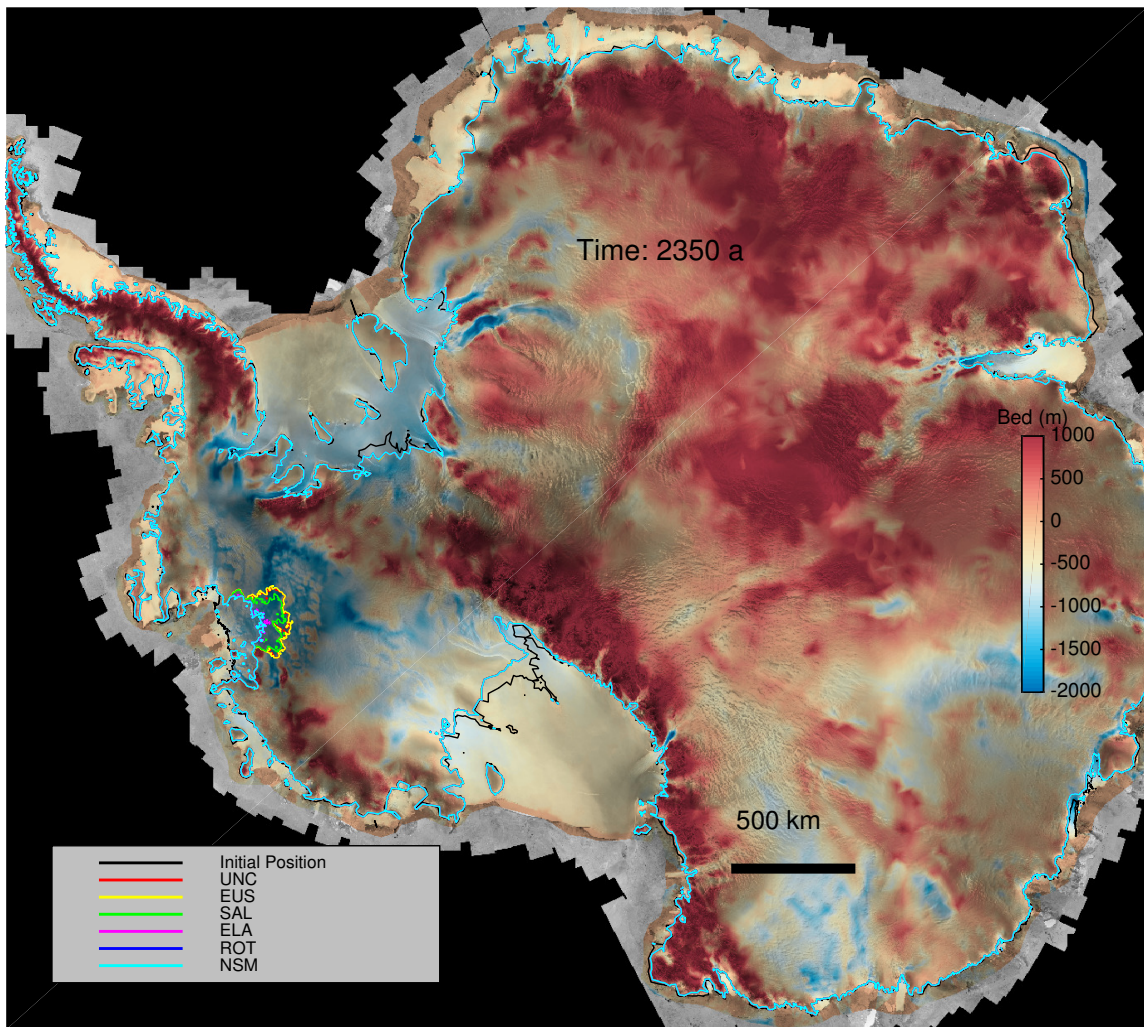


Fig. S4. Grounding-line projection for Antarctica at 2350. Results correspond to the six models defined in Table 1. The initial grounding line position in 2000 is shown in black. Grounding line positions are overlaid on a local bedrock topography of the continent (see Methods). Zooms on the areas of West Antarctica, Ronne Ice Shelf and Ross Ice Shelf are shown in Figures 4, S6 and S5 respectively.

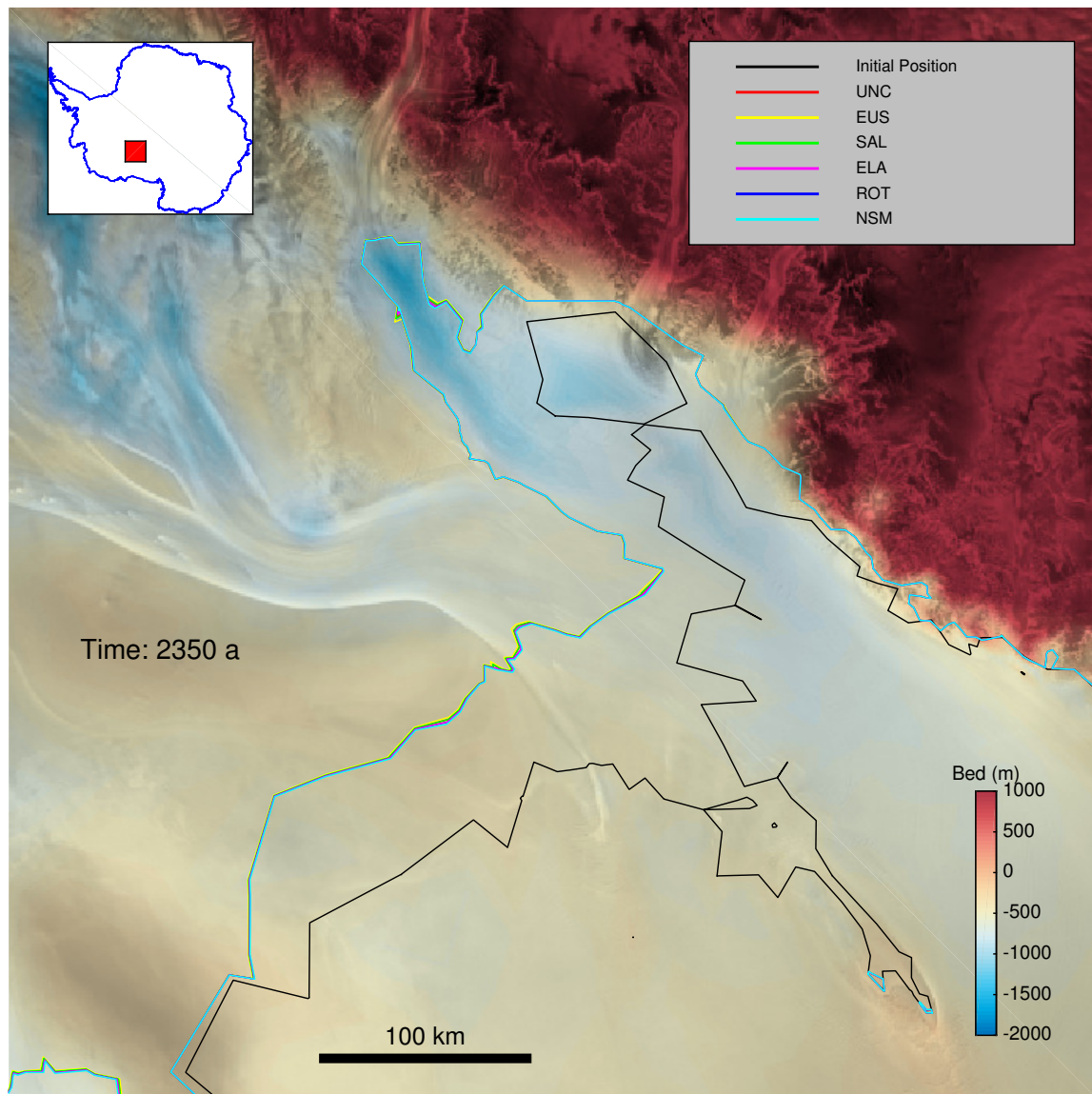


Fig. S5. Grounding-line projection for the Mercer Ice Stream (Ross Ice Shelf) at 2350. Results correspond to the six models defined in Table 1. The initial grounding line position in 2000 is shown in black. Grounding line positions are overlaid on a local bedrock topography map (see Methods). General location of the area within Antarctica is given in the upper left inset.

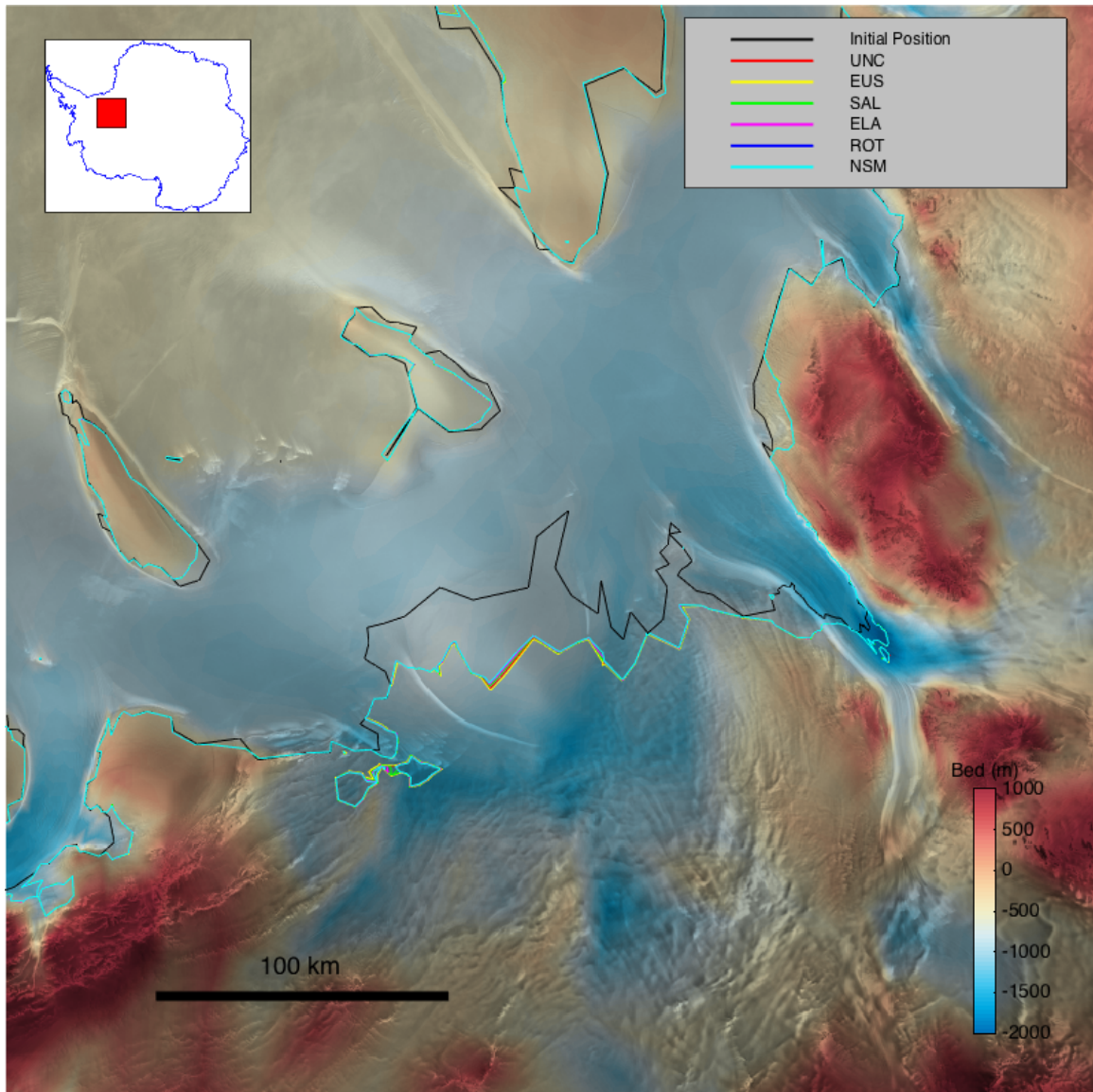


Fig. S6. Grounding-line projection for Ronne Ice Shelf at 2350. Results correspond to the six models defined in Table 1. The initial grounding line position in 2000 is shown in black. Grounding line positions are overlaid on a local bedrock topography map (see Methods). General location of the area within Antarctica is given in the upper left inset.

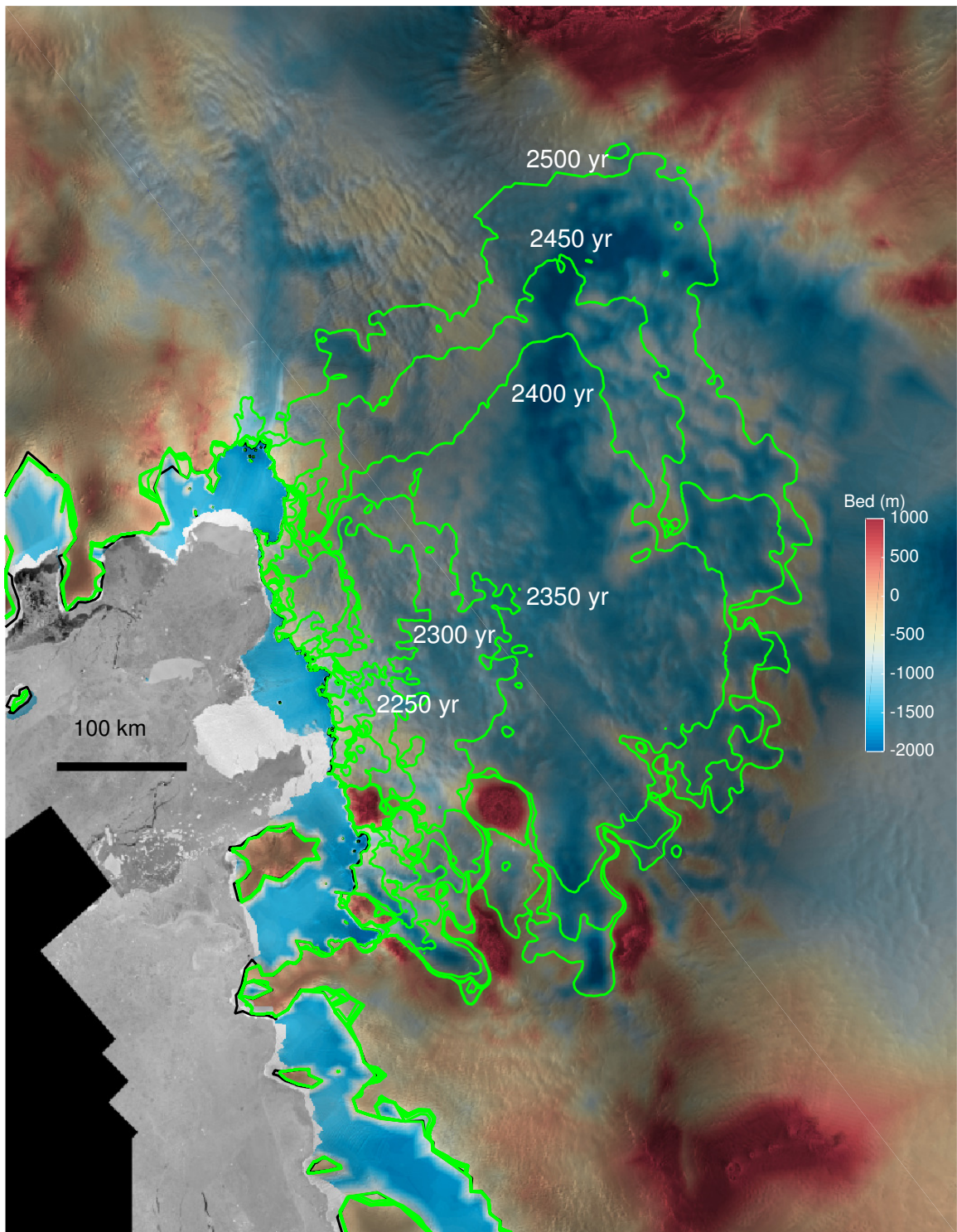


Fig. S7. Transient evolution of the TG grounding line from 2000 to 2500. Initial grounding line position is shown in black. Grounding line positions are overlaid over a bedrock topography map (see Methods). This run involves the NSM model. (see Table 1 for a description). Collapse of Thwaites Glacier starts in earnest at year 2300, initiating a grounding line retreat of 250 km in the span of 100 years.

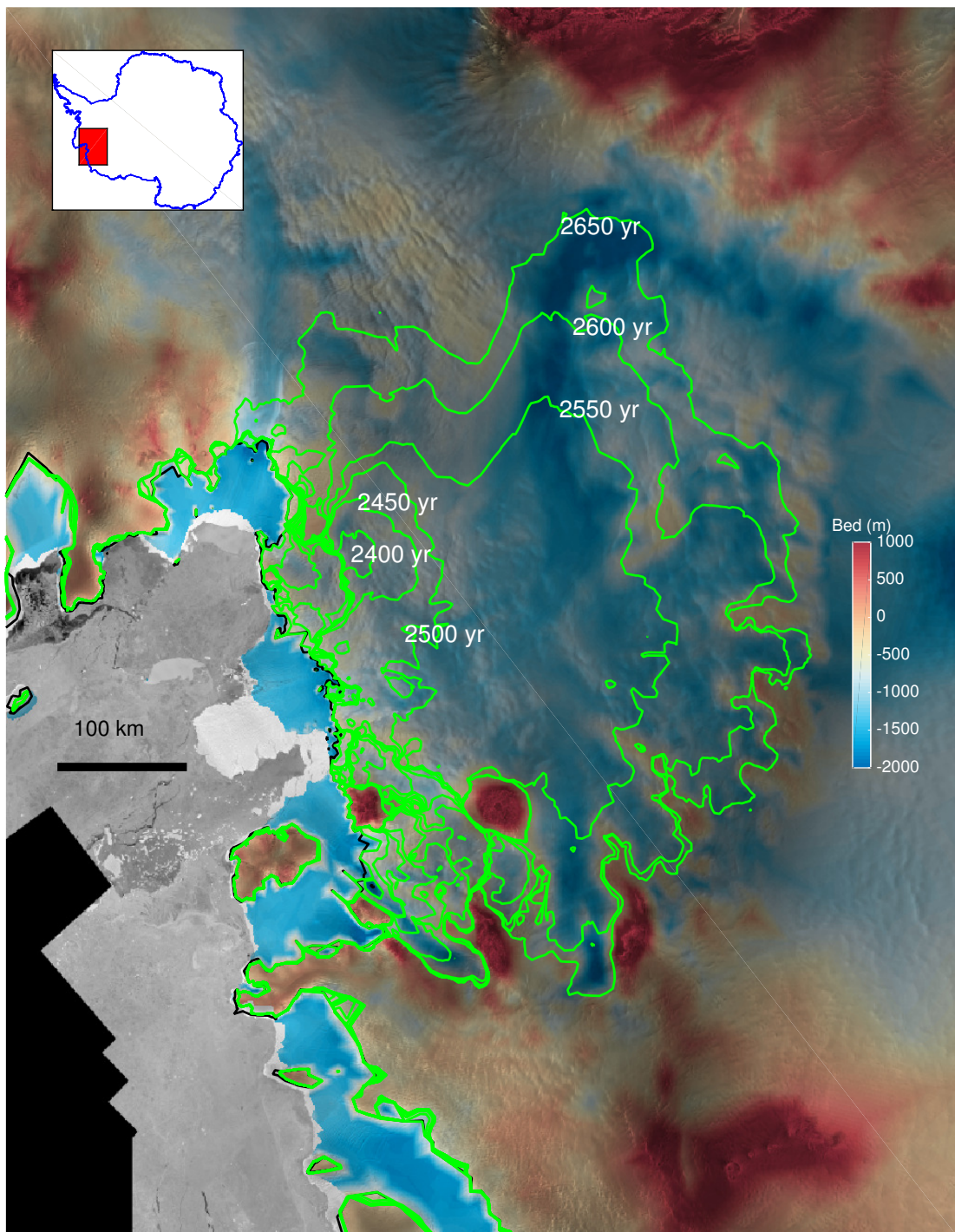


Fig. S8. Transient evolution of the TG grounding line from 2000 to 2500 using a coarser mesh. The results shown here are similar to the ones shown in Fig. S7 except that the mesh resolution for the underlying model is coarsened for TG from 1 km everywhere to a range of 1 km at the 2000 grounding line down to 8 km at the 2500 grounding line. The end result of this coarsening is a delay of 160 years in the overall grounding line retreat of TG.

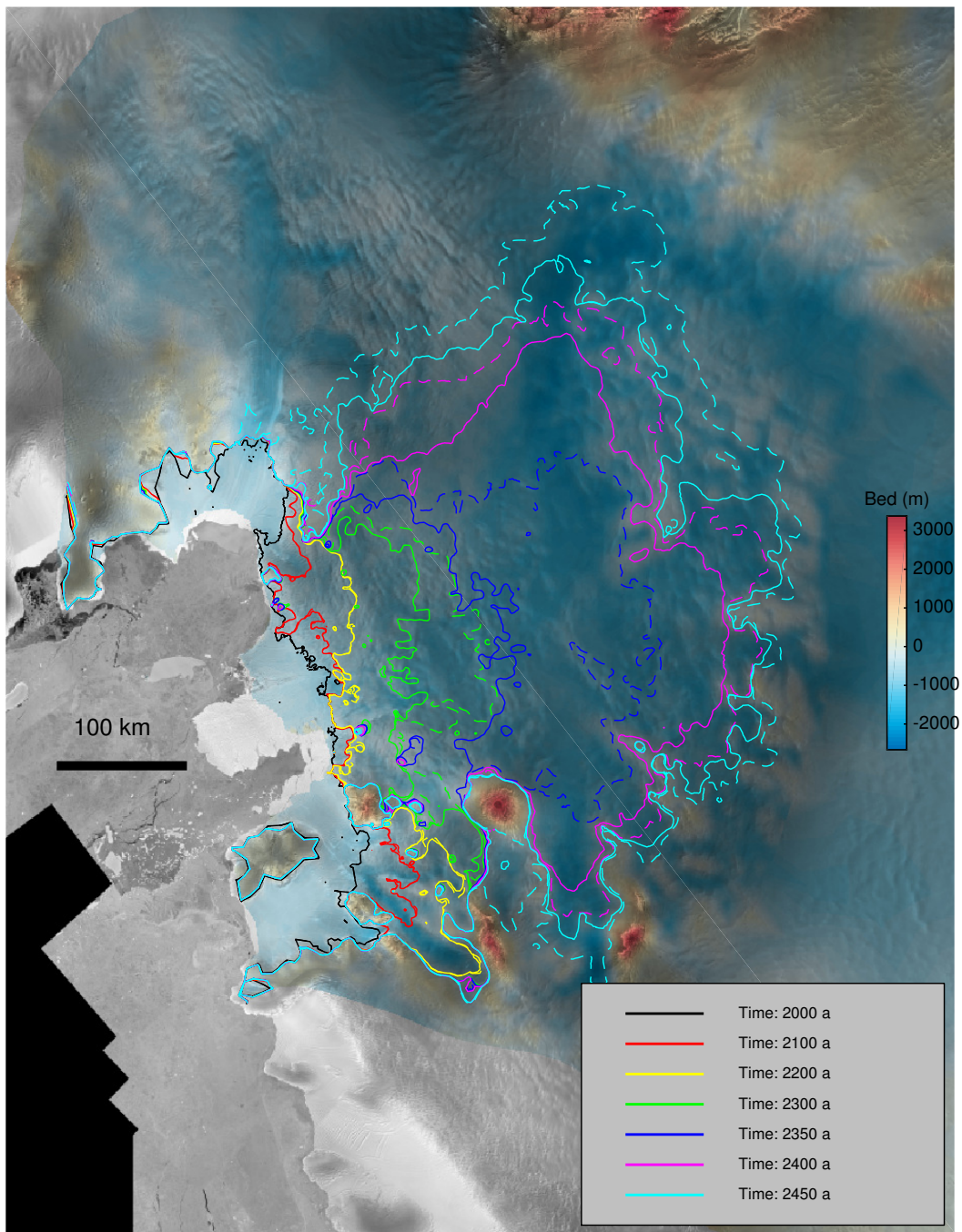


Fig. S9. Projection of grounding line retreat for TG and PIG. Full and dotted lines correspond to the UNC and NSM models respectively (see Table 1 for a definition of these models), plotted at 100 year time intervals (except for additional year 2350). Each color is coded for a time step provided in the legend. A maximum distance of approximately 120 km between both models occurs around 2350, during the retreat of Thwaites glacier Initial grounding line position is shown in black. Grounding line positions are overlaid over a bedrock topography map (see Methods).

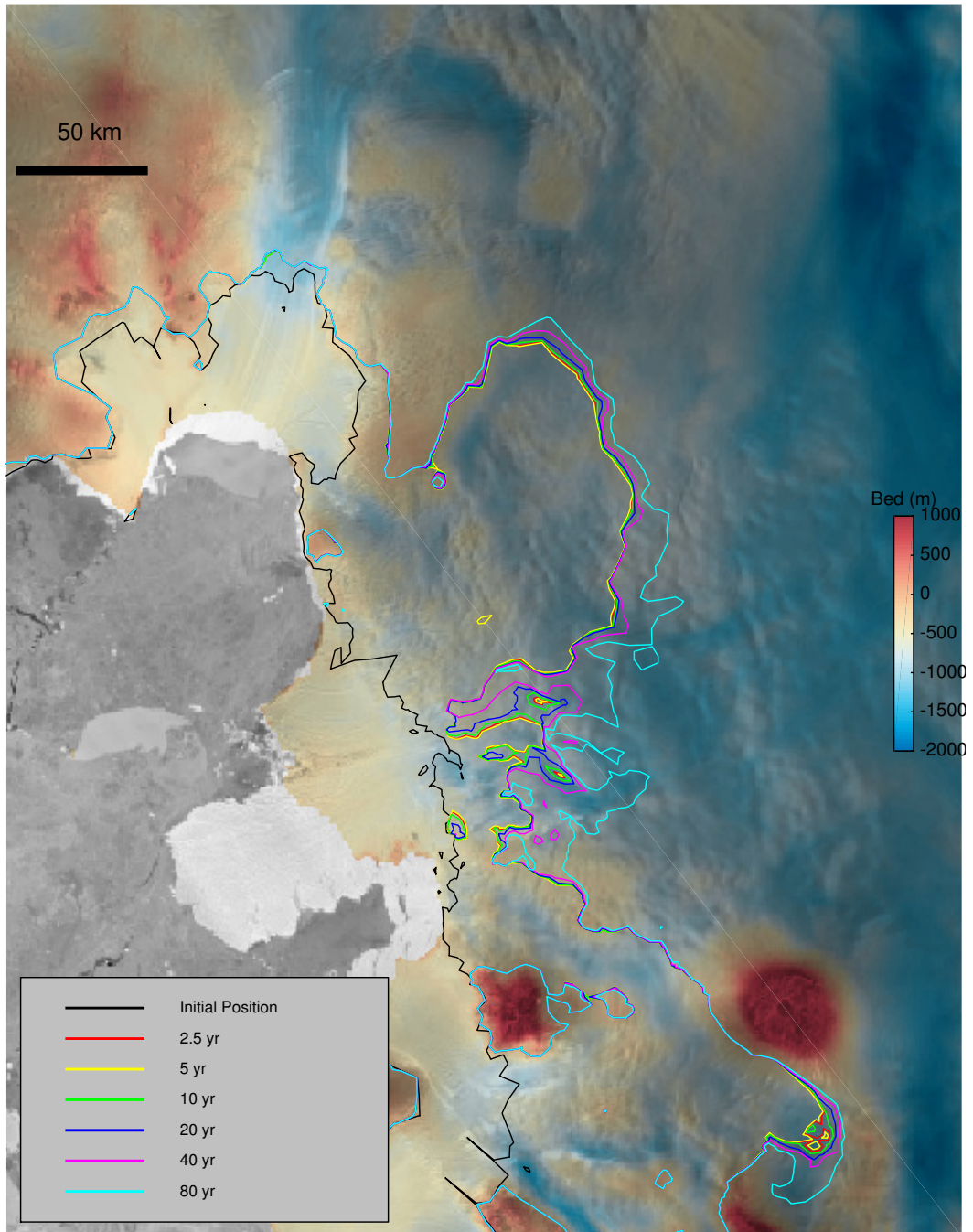


Fig. S10. Impact of sea-level solver time step on grounding line dynamics of TG and PIG, Antarctica. The simulation is based on the NSM model (see Table 1 for a definition) and a coarsened mesh resolution (1 km at the 2000 grounding line increased to 8 km at the 2500 grounding line). Projected grounding line position after 350 years is shown for different time steps ranging from 2.5 yr to 80 yr. The increasing separation between each grounding line position with increasing time steps suggest a time step of 5 years or lower is required to achieve convergence of the two-way RSL/ice-flow solver. Initial grounding line position is shown in black. Grounding line positions are overlaid over a bedrock topography map (see Methods).

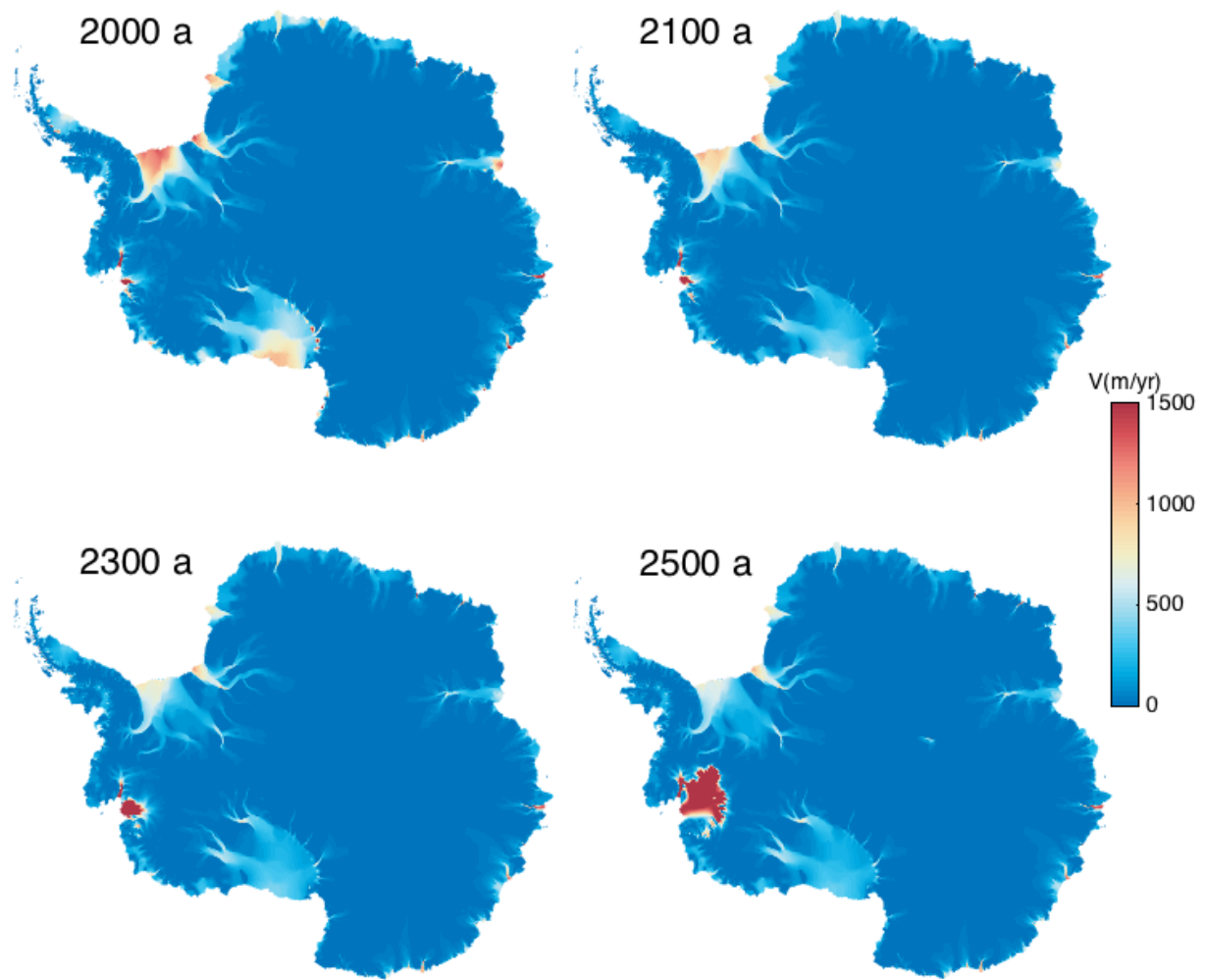


Fig. S11. Projected evolution of Antarctica surface velocity (in m/yr) from 2000 to 2500. The simulation involves the NSM model (see Table 1 for description). Dynamic retreat of TG (resulting in increased surface velocity following grounding line retreat and dynamic thinning) initiates around 2250, and is in full motion by 2500.

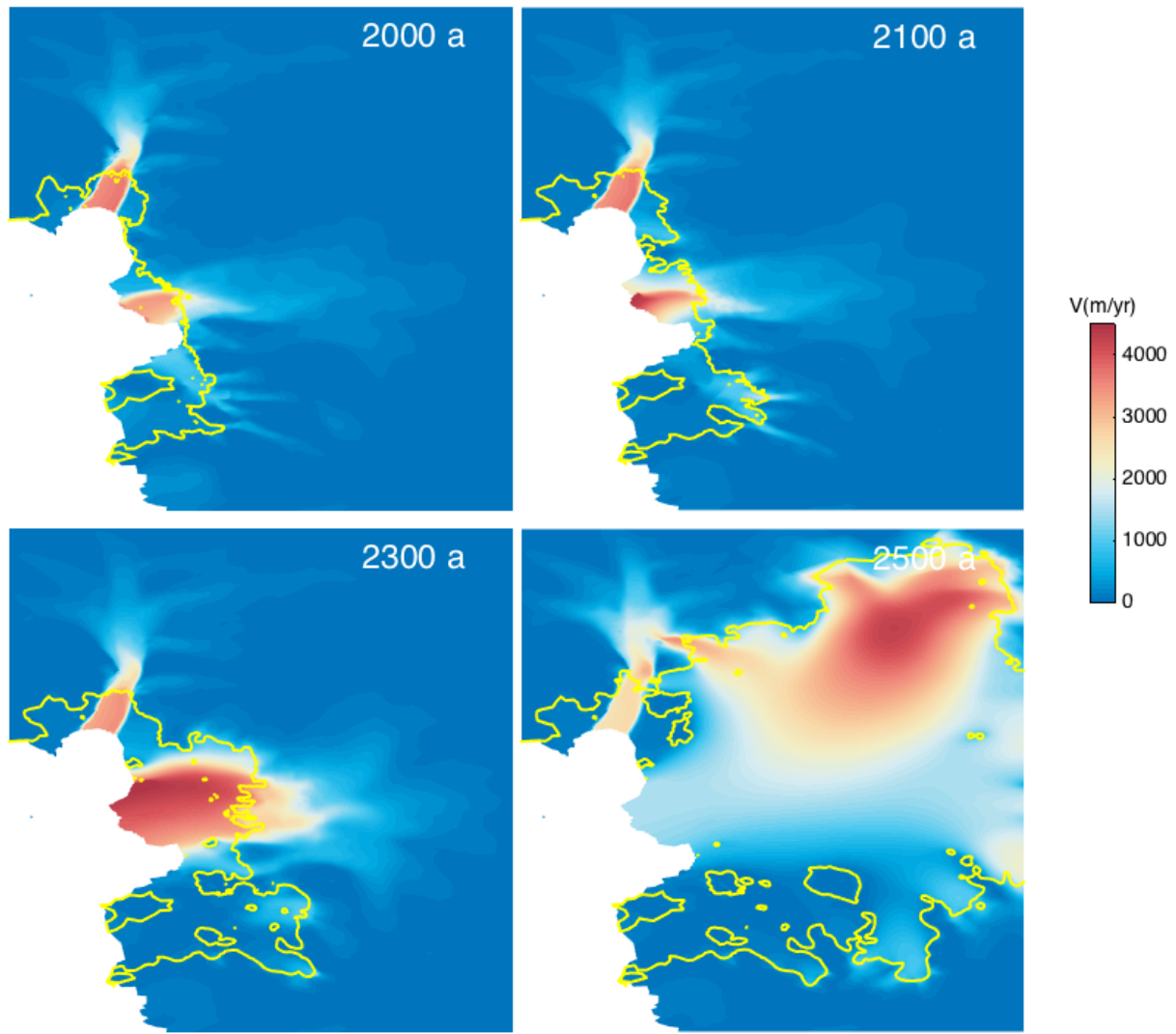


Fig. S12. Projected evolution of surface velocity (in m/yr) of TG and PIG from 2000 to 2500. The simulation involves the NSM model (see Table 1 for description). Grounding line positions for each time step are marked in yellow.

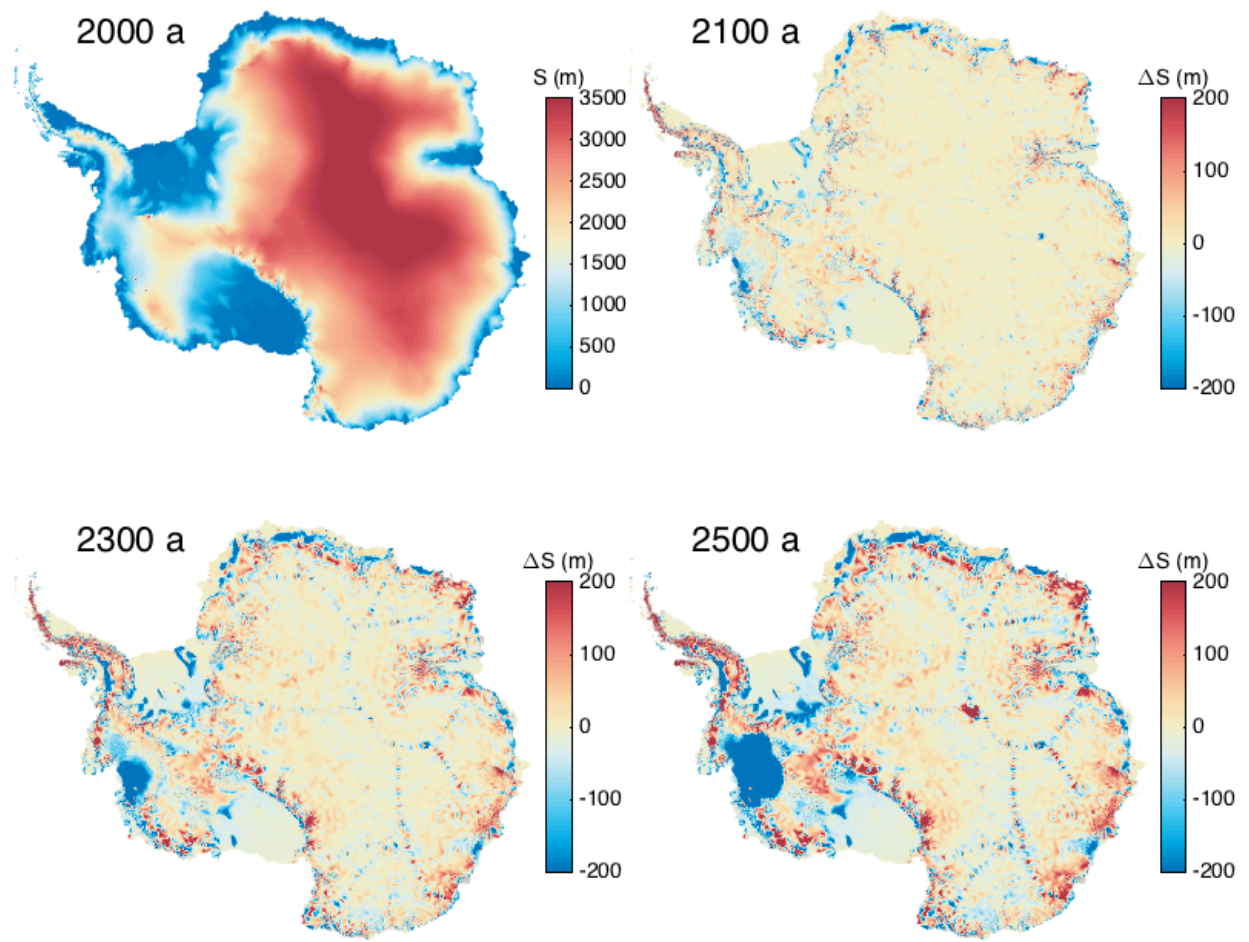


Fig. S13. Modeled evolution of Antarctica surface elevation (in m) from 2000 to 2500. The simulation involves the NSM model (see Table 1 for description). The initial elevation is displayed for year 2000, along with incremental changes (ΔS in m) for years 2100, 2300 and 2500. Dynamic thinning during the collapse of Thwaites Glacier initiates in year 2250, and is clearly visible by year 2500.

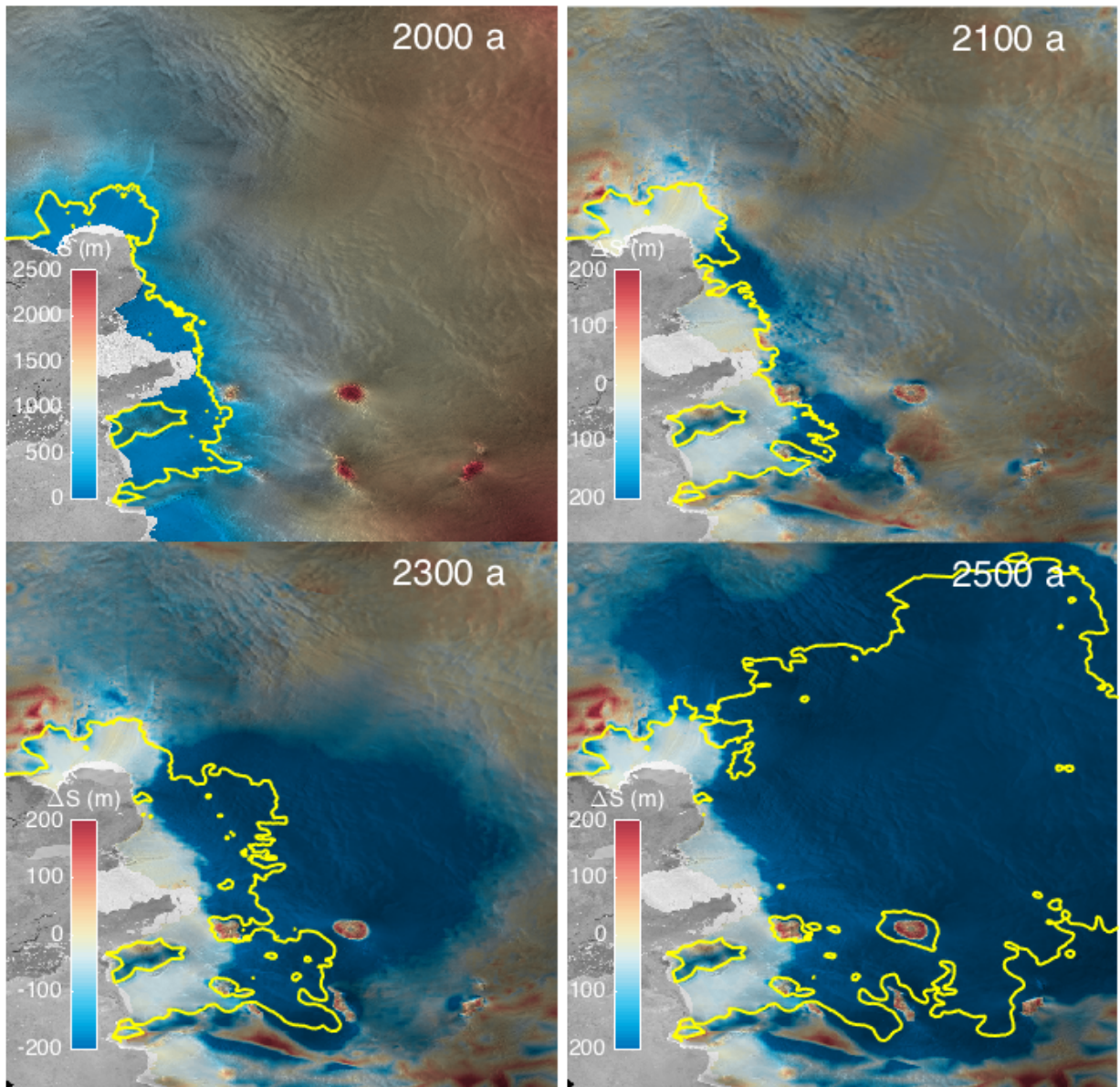


Fig. S14. Projected evolution of WAIS surface elevation (in m) from 2000 to 2500.
 The simulation involves the NSM model (see Table 1 for description). The initial elevation is displayed for year 2000, along with incremental changes (ΔS in m) for years 2100, 2300 and 2500. Grounding line positions for each time step are marked in yellow.

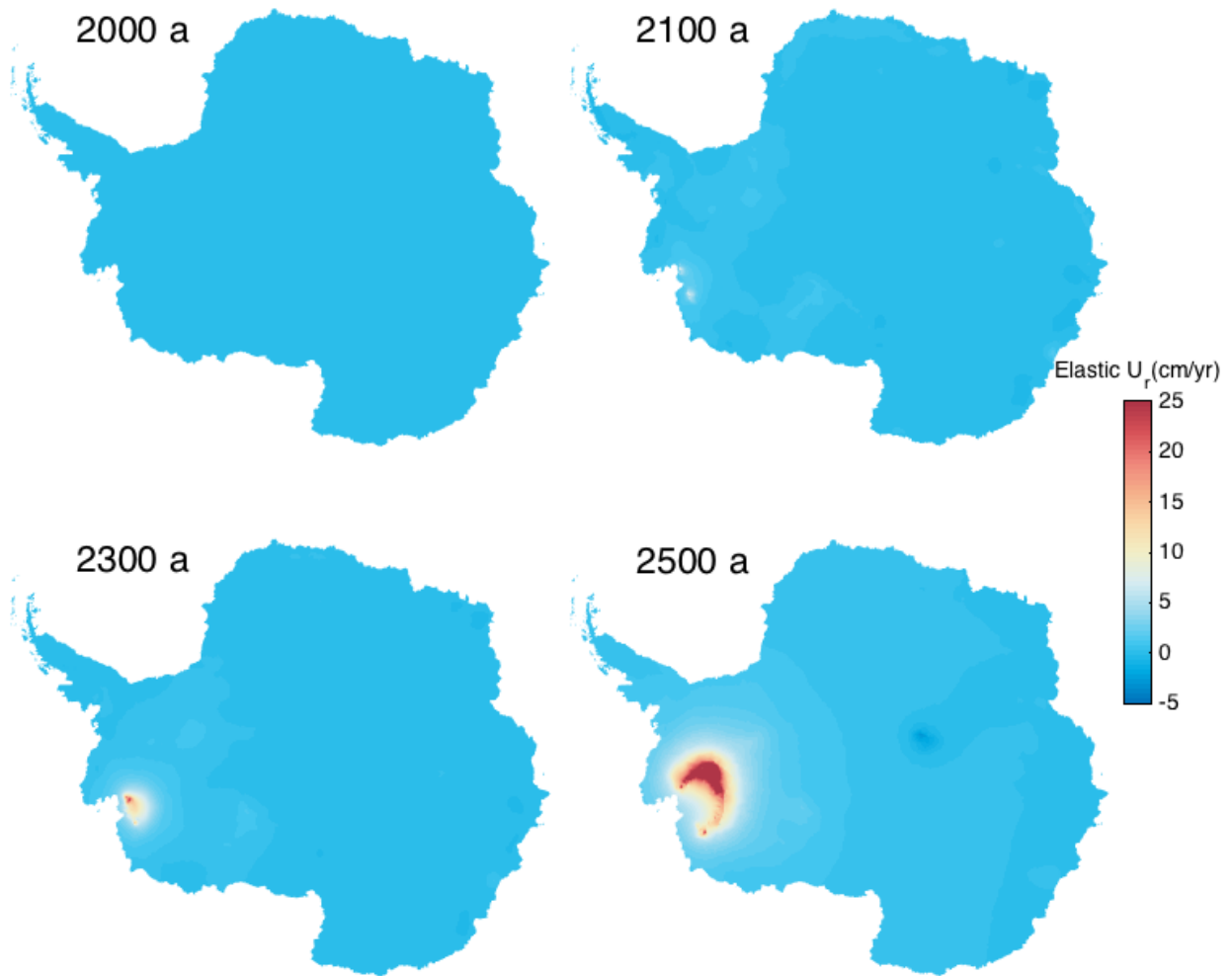


Fig. S15. Projected evolution of Antarctica elastic uplift U_r (in cm/yr) from 2000 to 2500. The simulation involves the NSM model (see Table 1 for description).

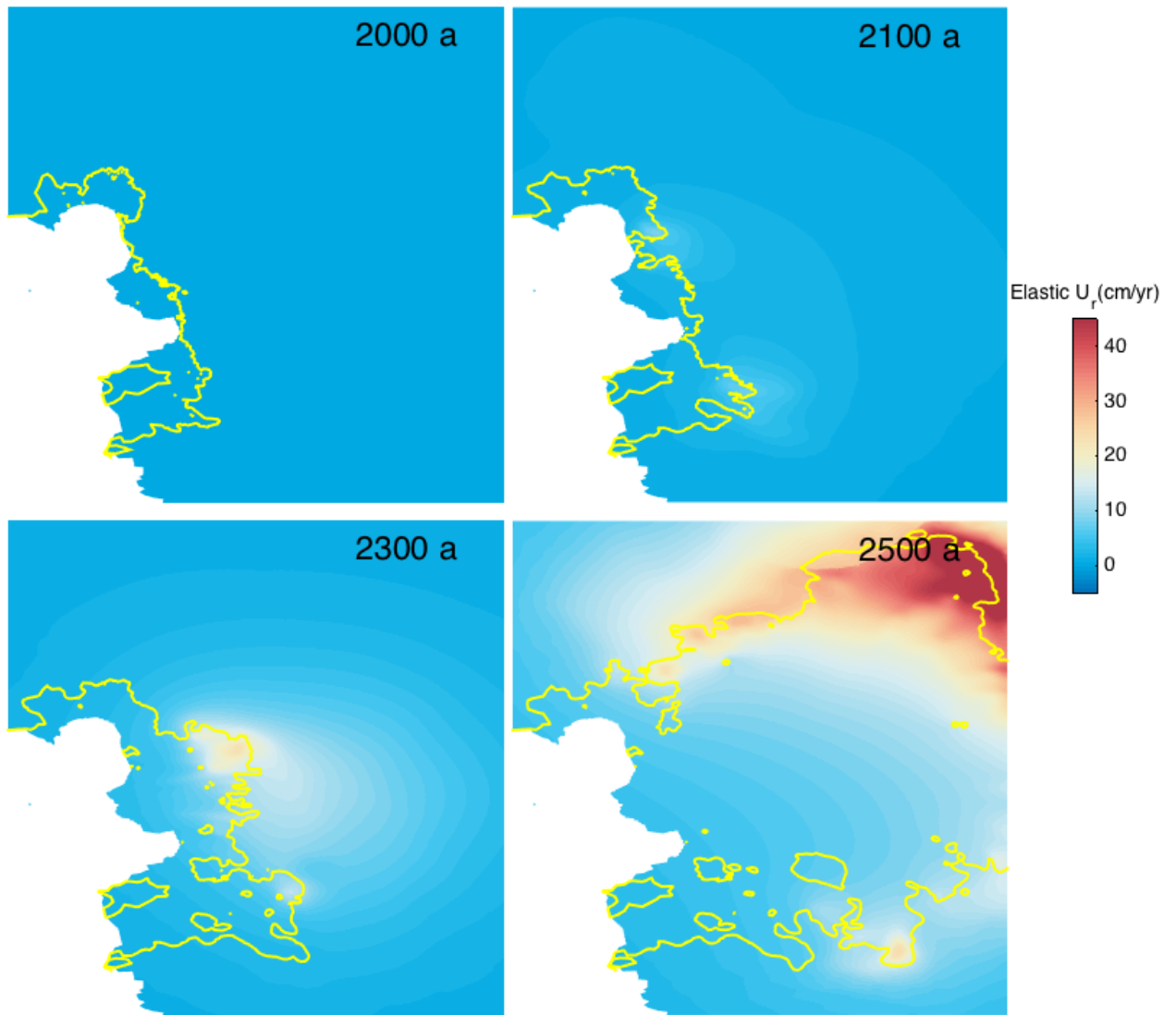


Fig. S16. **Projected evolution of WAIS elastic uplift U_r (in cm/yr) from 2000 to 2500.**
See Fig. S15 for details.

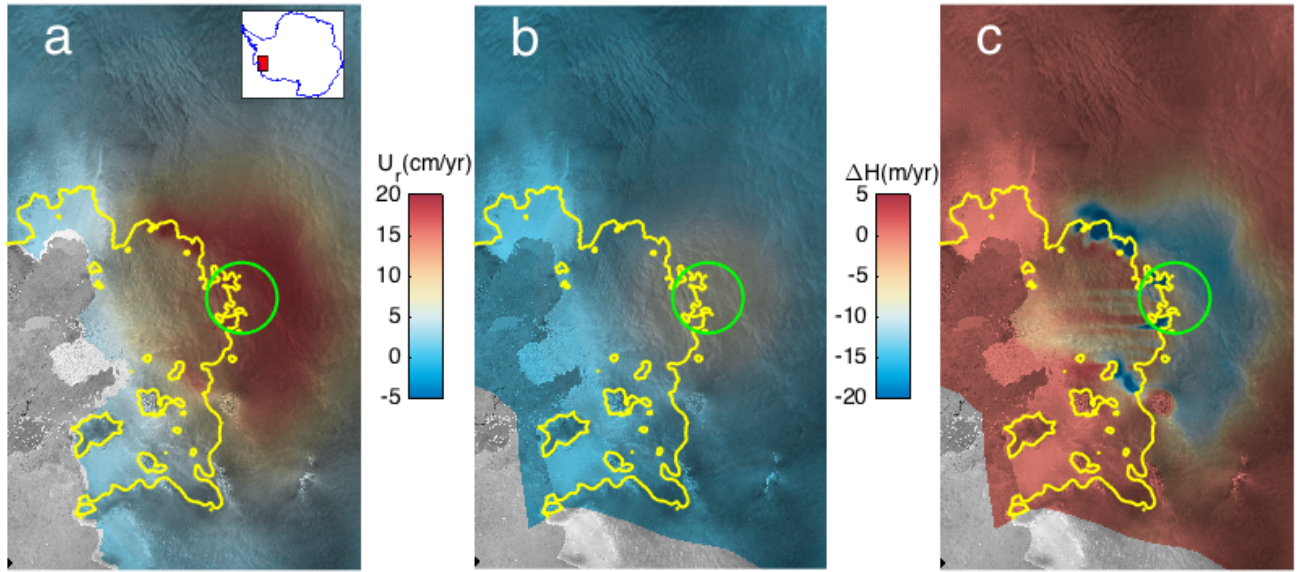


Fig. S17. Validation of projected elastic uplift rate U_r (in cm/yr) against the deformation benchmark (36) at 2350. Frame a: uplift rate U_r 350 years into the future for the WAIS area. Frame b: elastic uplift rate (in cm/yr) modeled using the benchmark for a 50 km radius disk loaded using projections of ice thickness change (frame c) corresponding to the same area. Frame c: projected ice thickness change rate (in m/yr) 350 years into the future. This thickness change rate is injected into the benchmark in frame b) to load the 50 km radius disk. Grounding line positions are marked in yellow.

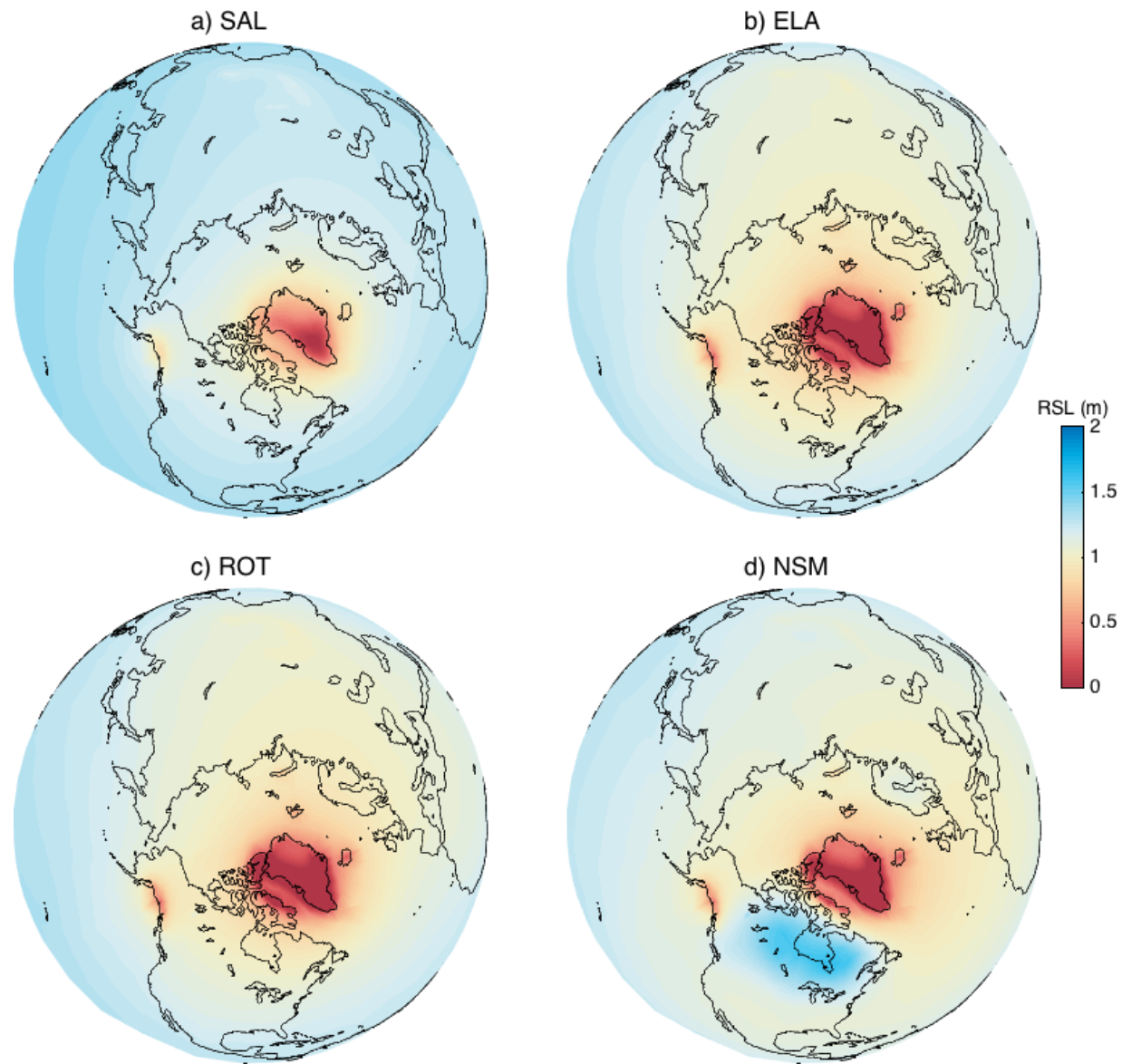


Fig. S18. **RSL projection at 2350.** This figure is similar to Figure 3 except for the view of the globe which corresponds to an azimuth of 0° and elevation of 90° .

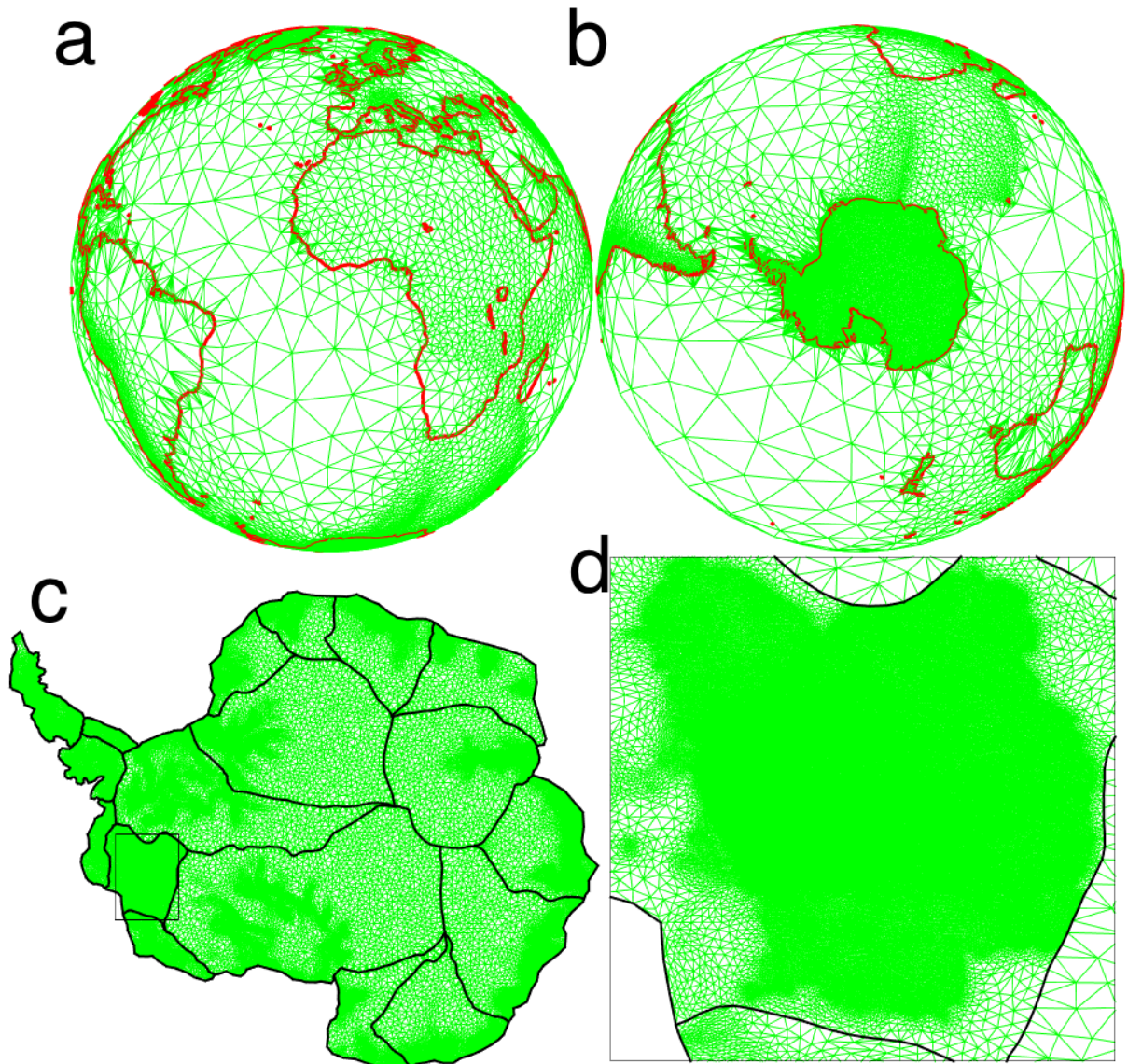


Fig. S19. Unstructured mesh used for modeling the evolution of global RSL and ice-flow in Antarctica. Meshing is carried out in an unstructured way to accommodate the ISSM SeSAW solver, with a resolution ranging from 1600 km (elements of the Atlantic and Pacific oceans) to 1 km (in the WAIS area, see frame c and d). For Antarctica, mesh resolution is significantly increased to be compatible with the ISSM Finite Element ice-flow solver (maximum of 25 km, minimum of 1 km). Meshing is carried out over 18 delimited basins (see frame c, each basin border marked in black) all connected together and coincident with the global mesh. A zoom on the WAIS area (frame d) is shown, with resolution increased to 1 km in the upstream areas of TG and PIG where grounding line occurs in the first 500 years of the simulation. For more details on how the ISSM ice-flow solver and ISSM SeSAW sea-level solver are run on this mesh, we refer to Methods.

References and Notes

1. W. E. Farrell, J. A. Clark, On Postglacial Sea Level. *Geophys. J. Int.* **46**, 647–667 (1976).
[doi:10.1111/j.1365-246X.1976.tb01252.x](https://doi.org/10.1111/j.1365-246X.1976.tb01252.x)
2. K. Lambeck, The Earth's variable rotation, Geophysical Causes and Consequences (Cambridge University Press, Cambridge, 2009).
3. W. R. Peltier, The impulse response of a Maxwell Earth. *Rev. Geophys.* **12**, 649 (1974).
[doi:10.1029/RG012i004p00649](https://doi.org/10.1029/RG012i004p00649)
4. N. Gomez, J. X. Mitrovica, M. E. Tamisiea, P. U. Clark, A new projection of sea level change in response to collapse of marine sectors of the Antarctic Ice Sheet. *Geophys. J. Int.* **180**, 623–634 (2010). [doi:10.1111/j.1365-246X.2009.04419.x](https://doi.org/10.1111/j.1365-246X.2009.04419.x)
5. N. Gomez, J. X. Mitrovica, P. Huybers, P. U. Clark, Sea level as a stabilizing factor for marine-ice-sheet grounding lines. *Nat. Geosci.* **3**, 850–853 (2010). [doi:10.1038/ngeo1012](https://doi.org/10.1038/ngeo1012)
6. S. Adhikari, E. R. Ivins, E. Larour, H. Seroussi, M. Morlighem, S. Nowicki, Future Antarctic bed topography and its implications for ice sheet dynamics. *Solid Earth* **5**, 569–584 (2014).
[doi:10.5194/se-5-569-2014](https://doi.org/10.5194/se-5-569-2014)
7. H. Konrad, I. Sasgen, D. Pollard, V. Klemann, Potential of the solid-Earth response for limiting long-term West Antarctic Ice Sheet retreat in a warming climate. *Earth Planet. Sci. Lett.* **432**, 254–264 (2015). [doi:10.1016/j.epsl.2015.10.008](https://doi.org/10.1016/j.epsl.2015.10.008)
8. V. R. Barletta, M. Bevis, B. E. Smith, T. Wilson, A. Brown, A. Bordoni, M. Willis, S. A. Khan, M. Rovira-Navarro, I. Dalziel, R. Smalley Jr., E. Kendrick, S. Konfal, D. J. Caccamise 2nd, R. C. Aster, A. Nyblade, D. A. Wiens, Observed rapid bedrock uplift in Amundsen Sea Embayment promotes ice-sheet stability. *Science* **360**, 1335–1339 (2018).
[doi:10.1126/science.aao1447](https://doi.org/10.1126/science.aao1447) [Medline](#)
9. J. Kingslake, R. P. Scherer, T. Albrecht, J. Coenen, R. D. Powell, R. Reese, N. D. Stansell, S. Tulaczyk, M. G. Wearing, P. L. Whitehouse, Extensive retreat and re-advance of the West Antarctic Ice Sheet during the Holocene. *Nature* **558**, 430–434 (2018). [doi:10.1038/s41586-018-0208-x](https://doi.org/10.1038/s41586-018-0208-x) [Medline](#)
10. E. Rignot, J. Mouginot, M. Morlighem, H. Seroussi, B. Scheuchl, Widespread, rapid grounding line retreat of Pine Island, Thwaites, Smith, and Kohler glaciers, West Antarctica, from 1992 to 2011. *Geophys. Res. Lett.* **41**, 3502–3509 (2014). [doi:10.1002/2014GL060140](https://doi.org/10.1002/2014GL060140)
11. H. Seroussi, Y. Nakayama, E. Larour, D. Menemenlis, M. Morlighem, E. Rignot, A. Khazendar, Continued retreat of Thwaites Glacier, West Antarctica, controlled by bed topography and ocean circulation. *Geophys. Res. Lett.* **44**, 6191–6199 (2017).
[doi:10.1002/2017GL072910](https://doi.org/10.1002/2017GL072910)
12. E. Rignot, J. Mouginot, B. Scheuchl, Ice flow of the Antarctic ice sheet. *Science* **333**, 1427–1430 (2011). [doi:10.1126/science.1208336](https://doi.org/10.1126/science.1208336) [Medline](#)
13. L. Favier, G. Durand, S. L. Cornford, G. H. Gudmundsson, O. Gagliardini, F. Gillet-Chaulet, T. Zwinger, A. J. Payne, A. M. Le Brocq, Retreat of Pine Island Glacier controlled by marine ice-sheet instability. *Nat. Clim. Chang.* **4**, 117–121 (2014). [doi:10.1038/nclimate2094](https://doi.org/10.1038/nclimate2094)
14. K. Matsuoka, R. C. A. Hindmarsh, G. Moholdt, M. J. Bentley, H. D. Pritchard, J. Brown, H. Conway, R. Drews, G. Durand, D. Goldberg, T. Hattermann, J. Kingslake, J. T. M. Lenaerts, C. Martín, R. Mulvaney, K. W. Nicholls, F. Pattyn, N. Ross, T. Scambos, P. L. Whitehouse, Antarctic ice rises and ripples: Their properties and significance for ice-sheet dynamics and evolution. *Earth Sci. Rev.* **150**, 724–745 (2015).
[doi:10.1016/j.earscirev.2015.09.004](https://doi.org/10.1016/j.earscirev.2015.09.004)

15. G. H. Gudmundsson, J. Krug, G. Durand, L. Favier, O. Gagliardini, The stability of grounding lines on retrograde slopes. *Cryosphere* **6**, 1497–1505 (2012). [doi:10.5194/tc-6-1497-2012](https://doi.org/10.5194/tc-6-1497-2012)
16. S. Anandakrishnan, D. D. Blankenship, R. B. Alley, P. L. Stoffa, Influence of subglacial geology on the position of a West Antarctic ice stream from seismic observations. *Nature* **394**, 62–65 (1998). [doi:10.1038/27889](https://doi.org/10.1038/27889)
17. E. J. Rignot, Fast recession of a west antarctic glacier. *Science* **281**, 549–551 (1998). [doi:10.1126/science.281.5376.549](https://doi.org/10.1126/science.281.5376.549) Medline
18. I. Joughin, B. E. Smith, B. Medley, Marine ice sheet collapse potentially under way for the Thwaites Glacier Basin, West Antarctica. *Science* **344**, 735–738 (2014). [doi:10.1126/science.1249055](https://doi.org/10.1126/science.1249055) Medline
19. F. Pattyn, L. Perichon, G. Durand, L. Favier, O. Gagliardini, R. C. A. Hindmarsh, T. Zwinger, T. Albrecht, S. Cornford, D. Docquier, J. J. Fürst, D. Goldberg, G. H. Gudmundsson, A. Humbert, M. Hütten, P. Huybrechts, G. Jouvet, T. Kleiner, E. Larour, D. Martin, M. Morlighem, A. J. Payne, D. Pollard, M. Rückamp, O. Rybak, H. Seroussi, M. Thoma, N. Wilkens, Grounding-line migration in plan-view marine ice-sheet models: Results of the ice2sea MISMIP3d intercomparison. *J. Glaciol.* **59**, 410–422 (2013). [doi:10.3189/2013JoG12J129](https://doi.org/10.3189/2013JoG12J129)
20. H. Konrad, I. Sasgen, D. Pollard, V. Klemann, Potential of the solid-Earth response for limiting long-term West Antarctic Ice Sheet retreat in a warming climate. *Earth Planet. Sci. Lett.* **432**, 254–264 (2015). [doi:10.1016/j.epsl.2015.10.008](https://doi.org/10.1016/j.epsl.2015.10.008)
21. B. de Boer, P. Stocchi, P. L. Whitehouse, R. S. W. van de Wal, Current state and future perspectives on coupled ice-sheet – sea-level modelling. *Quat. Sci. Rev.* **169**, 13–28 (2017). [doi:10.1016/j.quascirev.2017.05.013](https://doi.org/10.1016/j.quascirev.2017.05.013)
22. C. C. Hay, H. C. P. Lau, N. Gomez, J. Austermann, E. Powell, J. X. Mitrovica, K. Latychev, D. A. Wiens, Sea Level Fingerprints in a Region of Complex Earth Structure: The Case of WAIS. *J. Clim.* **30**, 1881–1892 (2017). [doi:10.1175/JCLI-D-16-0388.1](https://doi.org/10.1175/JCLI-D-16-0388.1)
23. R. Bindschadler, S. Nowicki, A. Abe-Ouchi, A. Aschwanden, H. Choi, J. Fastook, G. Granzow, R. Greve, G. Gutowski, U. Herzfeld, C. Jackson, J. Johnson, C. Khroulev, A. Levermann, W. H. Lipscomb, M. A. Martin, M. Morlighem, B. R. Parizek, D. Pollard, S. F. Price, D. Ren, F. Saito, T. Sato, H. Seddik, H. Seroussi, K. Takahashi, R. Walker, W. L. Wang, Ice-sheet model sensitivities to environmental forcing and their use in projecting future sea level (the SearISE project). *J. Glaciol.* **59**, 195–224 (2013). [doi:10.3189/2013JoG12J125](https://doi.org/10.3189/2013JoG12J125)
24. J. Weertman, Stability of the Junction of an Ice Sheet and an Ice Shelf. *J. Glaciol.* **13**, 3 (1974). [doi:10.1017/S002214300023327](https://doi.org/10.1017/S002214300023327)
25. G. A. Milne, J. X. Mitrovica, Postglacial sea-level change on a rotating Earth. *Geophys. J. Int.* **133**, 1–19 (1998). [doi:10.1046/j.1365-246X.1998.1331455.x](https://doi.org/10.1046/j.1365-246X.1998.1331455.x)
26. E. Larour, E. R. Ivins, S. Adhikari, Should coastal planners have concern over where land ice is melting? *Sci. Adv.* **3**, e1700537 (2017). [doi:10.1126/sciadv.1700537](https://doi.org/10.1126/sciadv.1700537) Medline
27. L. Caron, E. R. Ivins, E. Larour, S. Adhikari, J. Nilsson, G. Blewitt, GIA Model Statistics for GRACE Hydrology, Cryosphere, and Ocean Science. *Geophys. Res. Lett.* **45**, 2203–2212 (2018). [doi:10.1002/2017GL076644](https://doi.org/10.1002/2017GL076644)
28. E. Larour, H. Seroussi, M. Morlighem, E. Rignot, *J. Geophys. Res.* **117**, F01022 (2012).
29. S. Adhikari, E. R. Ivins, E. Larour, ISSM-SESAW v1.0: Mesh-based computation of gravitationally consistent sea-level and geodetic signatures caused by cryosphere and

climate driven mass change. *Geosci. Model Dev.* **9**, 1087–1109 (2016). [doi:10.5194/gmd-9-1087-2016](https://doi.org/10.5194/gmd-9-1087-2016)

30. S. Adhikari, E. R. Ivins, Climate-driven polar motion: 2003–2015. *Sci. Adv.* **2**, e1501693 (2016). [doi:10.1126/sciadv.1501693](https://doi.org/10.1126/sciadv.1501693) [Medline](#)
31. J. L. Bamber, R. E. M. Riva, B. L. A. Vermeersen, A. M. LeBrocq, Reassessment of the potential sea-level rise from a collapse of the West Antarctic Ice Sheet. *Science* **324**, 901–903 (2009). [doi:10.1126/science.1169335](https://doi.org/10.1126/science.1169335) [Medline](#)
32. J. X. Mitrovica, N. Gomez, P. U. Clark, The sea-level fingerprint of West Antarctic collapse. *Science* **323**, 753 (2009). [doi:10.1126/science.1166510](https://doi.org/10.1126/science.1166510) [Medline](#)
33. S. Nowicki *et al.*, *J. Geophys. Res.* **118**, 1 (2013).
34. S. M. J. Nowicki, T. Payne, E. Larour, H. Seroussi, H. Goelzer, W. Lipscomb, J. Gregory, A. Abe-Ouchi, A. Shepherd, Ice Sheet Model Intercomparison Project (ISMIP6) contribution to CMIP6. *Geosci. Model Dev.* **9**, 4521–4545 (2016). [doi:10.5194/gmd-9-4521-2016](https://doi.org/10.5194/gmd-9-4521-2016) [Medline](#)
35. M. P. Schodlok, D. Menemenlis, E. J. Rignot, Ice shelf basal melt rates around Antarctica from simulations and observations. *J. Geophys. Res. Oceans* **121**, 1085–1109 (2016). [doi:10.1002/2015JC011117](https://doi.org/10.1002/2015JC011117)
36. G. Spada, V. R. Barletta, V. Klemann, R. E. M. Riva, Z. Martinec, P. Gasperini, B. Lund, D. Wolf, L. L. A. Vermeersen, M. A. King, A benchmark study for glacial isostatic adjustment codes. *Geophys. J. Int.* **185**, 106–132 (2011). [doi:10.1111/j.1365-246X.2011.04952.x](https://doi.org/10.1111/j.1365-246X.2011.04952.x)
37. R. M. DeConto, D. Pollard, Contribution of Antarctica to past and future sea-level rise. *Nature* **531**, 591–597 (2016). [doi:10.1038/nature17145](https://doi.org/10.1038/nature17145) [Medline](#)
38. C. Ritz, T. L. Edwards, G. Durand, A. J. Payne, V. Peyaud, R. C. Hindmarsh, Potential sea-level rise from Antarctic ice-sheet instability constrained by observations. *Nature* **528**, 115–118 (2015). [Medline](#)
39. Past Interglacials Working Group of PAGES, Interglacials of the last 800,000 years. *Rev. Geophys.* **54**, 162–219 (2016). [doi:10.1002/2015RG000482](https://doi.org/10.1002/2015RG000482)
40. W. van der Wal, P. L. Whitehouse, E. J. Schrama, Effect of GIA models with 3D composite mantle viscosity on GRACE mass balance estimates for Antarctica. *Earth Planet. Sci. Lett.* **414**, 134–143 (2015). [doi:10.1016/j.epsl.2015.01.001](https://doi.org/10.1016/j.epsl.2015.01.001)
41. P. Wessel, W. H. F. Smith, A global, self-consistent, hierarchical, high-resolution shoreline database. *J. Geophys. Res. Oceans* **101** (B4), 8741–8743 (1996). [doi:10.1029/96JB00104](https://doi.org/10.1029/96JB00104)
42. D. MacAyeal, Large-scale ice flow over a viscous basal sediment: Theory and application to ice stream B, Antarctica. *J. Geophys. Res.* **94** (B4), 4071–4087 (1989). [doi:10.1029/JB094iB04p04071](https://doi.org/10.1029/JB094iB04p04071)
43. J. T. M. Lenaerts, M. R. van den Broeke, W. J. van de Berg, E. van Meijgaard, P. Kuipers Munneke, A new, high-resolution surface mass balance map of Antarctica (1979–2010) based on regional atmospheric climate modeling. *Geophys. Res. Lett.* **39**, 1 (2012). [doi:10.1029/2011GL050713](https://doi.org/10.1029/2011GL050713)
44. M. Morlighem, E. Rignot, H. Seroussi, E. Larour, H. Ben Dhia, D. Aubry, A mass conservation approach for mapping glacier ice thickness. *Geophys. Res. Lett.* **38**, 1 (2011). [doi:10.1029/2011GL048659](https://doi.org/10.1029/2011GL048659)
45. E. Larour, M. Morlighem, H. Seroussi, J. Schiermeier, E. Rignot, *J. Geophys. Res. Earth Surf.* **117**, 1 (2012).

46. J. Glen, The creep of polycrystalline ice. *Proc. R. Soc. London Ser. A* **228**, 519–538 (1955).
[doi:10.1098/rspa.1955.0066](https://doi.org/10.1098/rspa.1955.0066)
47. E. Larour, E. Rignot, I. Joughin, D. Aubry, Rheology of the Ronne Ice Shelf, Antarctica, inferred from satellite radar interferometry data using an inverse control method. *Geophys. Res. Lett.* **32**, L05503 (2005). [doi:10.1029/2004GL021693](https://doi.org/10.1029/2004GL021693)
48. F. Pattyn, A new three-dimensional higher-order thermomechanical ice sheet model: Basic sensitivity, ice stream development, and ice flow across subglacial lakes. *J. Geophys. Res.* **108**, 2382 (2003). [doi:10.1029/2002JB002329](https://doi.org/10.1029/2002JB002329)